The effect of spatiotemporal displacement on the integration of shape information

Robert J. Green School of Psychological Science, The University of Western Australia, Perth, Australia

J. Edwin Dickinson School of Psychological Science, The University of Western Australia, Perth, Australia

David R. Badcock School of Psychological Science, The University of Western Australia, Perth, Australia

Within a natural scene it is not uncommon for an object's shape to be revealed over time. We investigated whether the same integration of shape information that happens around a fully visible contour also happens when that information is distributed over time. In a two-interval forced-choice task, observers discriminated between a radial frequency (RF) pattern and a circle that were revealed either using an implicit slit or traced out by a dot's motion; and a line and a modulated line that were either contour-defined or motion-defined. First, with presentation times of approximately 1 s, we found no difference in the strength of integration when comparing a freely visible contour to one that (a) moved behind a slit; (b) was revealed by a moving slit; or (c) revealed piecemeal by a slit appearing at random locations (Experiment 1). Changing the duration of presentation (250–4,000 ms) had no effect on strength of integration or threshold for detection within the moving slit condition (Experiment 2). Considering these results, Experiment 3 revisited integration for a dot tracing out an RF path (Or, Thabet, Wilkinson, & Wilson, 2011), finding removal of a change in speed cue increased the strength of integration to that found in Experiments 1 and 2 of the current study. The pattern of results for modulated lines was different from RF patterns; however, within these conditions, there was no difference in strength of integration between contour-defined and motion-defined stimuli. Our results suggest motion-defined patterns are processed as form from motion.

Introduction

Detection and discrimination of objects are important functions of the visual system, but not all objects within a scene are freely visible. Previous research has suggested that spatial disruption of contour information of a simple shape increases that shape's thresholds for detection (Hess, Wang, & Dakin, 1999; Loffler, Wilson, & Wilkinson, 2003) and that information cannot be integrated across discrete shapes (Baldwin, Schmidtmann, Kingdom, & Hess, 2016). It has been suggested that spatiotemporally tuned cells enable us to combine form information when an object moves behind a stationary slit (Burr & Ross, 2004) and indeed object recognition is easy under these circumstances (Yin, Shimojo, Moore, & Engel, 2002). However, there has not been much research on the effect of these viewing conditions on the integration of local orientation information around the contour of a simple shape.

The radial frequency (RF) pattern is a pattern that has frequently been used to assess integration of information around a simple contour. These patterns are derived from circles that have their radius sinusoidally modulated as a function of their polar angle. Their RF number is related to their wavelength, but usually defined by the number of cycles able to fill 2π radians. This is distinguished from the number of cycles (or lobes) present on the path, which is the number of complete sine waves within the pattern (see Figure 1). Increasing the amplitude of the sine wave increases the deformation and in turn, the probability of detection of the modulation.

There have been a variety of studies examining a number of different constraints on abilities to perceive and code shape information using RF patterns: global integration (Bell & Badcock, 2008; Dickinson, Han, Bell, & Badcock, 2010; Dickinson, McGinty, Webster, & Badcock, 2012; Hess et al., 1999; Loffler et al., 2003; Schmidtmann, Kennedy, Orbach, & Loffler, 2012; Tan, Bowden, Dickinson, & Badcock, 2015; Tan, Dickinson,

Citation: Green, R. J., Dickinson, J. E., & Badcock, D. R. (2018). The effect of spatiotemporal displacement on the integration of shape information. *Journal of Vision*, *18*(5):4, 1–18, https://doi.org/10.1167/18.5.4.

https://doi.org/10.1167/18.5.4 Received November 3, 2017; published May 2, 2018 ISSN 1534-7362

Figure 1. An RF3 with one, two, and three cycles of modulation (left to right). Amplitude ($A = 0.1$) of the patterns is well above threshold, but shown for illustrative purposes.

& Badcock, 2013), curvature (Dickinson, Cribb, Riddell, & Badcock, 2015), shape adaptation (Bell, Dickinson, & Badcock, 2008), polar angle between adjacent features (Dickinson, Bell, & Badcock, 2013), and size (Habak, Wilkinson, Zakher, & Wilson, 2004). In addition to these Or, Thabet, Wilkinson, and Wilson (2011) used a dot with a difference of Gaussians (DOG) luminance profile to trace out the path of a RF pattern over a period of 1 and 2 s. They concluded there was evidence for global integration of this motion RF pattern for both stimulus durations.

Evidence for global integration is determined by comparing the decrease in observer thresholds with increasing number of cycles of modulation to that predicted by probability summation (the increased likelihood of local feature detection due to the increase in number of local elements). The results of Or et al. (2011) suggest that global integration of shape information can occur over relatively long temporal periods, but it is unclear as to whether this is only possible for motion trajectories of stimuli or if it can also occur for a contour-defined shape presented over time. There is evidence from Schmidtmann et al. (2012) that may indicate simultaneous presentation of information is required, as they suggested that all cycles of modulation needed to be present to produce the reduction in deformation thresholds required for an RF pattern to demonstrate global processing. Their results, however, were not typical of previous research which finds a smooth decrease in observer thresholds with increasing cycles of modulation (Bell & Badcock, 2008; Dickinson et al., 2010; Dickinson et al., 2012; Loffler et al., 2003; Tan et al., 2013), not a "dog leg" as found by Schmidtmann et al. (2012).

Given that it is not uncommon for the natural scene to create a slit (an ajar door, two trees close together, long grass, etc.) through which we view a distal object, we will initially employ the use of a single slit to create temporal displacement of our contour-defined RF patterns and investigate the effect of presenting form information over time on global integration for spatially, temporally, and spatiotemporally distributed information.

Experiment 1

Methods

Observers

Five experienced psychophysical observers participated in the current experiment, three of whom were naïve to the experimental aims. All observers had normal or corrected-to-normal visual acuity, which was assessed using a LogMAR chart. Observers viewed stimuli binocularly, except for ED who has a divergent squint and completed the experiments under monocular viewing conditions using an opaque occluder (black eye patch).

Stimuli

The stimuli used were RF patterns as defined by Wilkinson, Wilson, and Habak (1998):

$$R(\theta) = R_0 \times [1 + A\sin(\omega\theta + \varphi)] \quad (1)$$

where θ is the angle created with the x axis, R_0 is the mean radius (30′ of visual angle in all conditions), A is the amplitude of modulation (proportion of mean radius), ω is the frequency of modulation (number of cycles per 2π radians), and φ is the phase of the sinusoidal modulation. Patterns containing less than the full three cycles of modulation used a D1 (first derivative of a Gaussian) function to replace the first half and last half cycle so they smoothly returned the contour to a circle (following Loffler et al., 2003). At one cycle of modulation, therefore, the modulated path conforms solely to a D1. The cross-section of the luminance profile conformed to a Gaussian with a sigma (σ) of 2′ of visual angle. Pilot testing found, after a number of trials, that observers had trouble maintaining the percept of an object in motion and, rather, perceived the stimulus as two points of light diverging and converging, a version of the aperture effect. To aid in their perception, a static textured pattern was applied to the stimulus by randomly choosing half the pixels every interval to be the same as the background luminance rather than that defined by the Gaussian luminance profile (see Figure 2). These pixels remained at the same spatial location on the contour during its presentation and gave the observer local cues that helped indicate the position of the contour over time and worked against the percept of smooth vertical motion of two dots.

Apparatus

Custom software in MATLAB 5.3 (MathWorks, Nantucket, MA; 1999) was used to create the stimuli, which were drawn to the screen of a Sony Trinitron

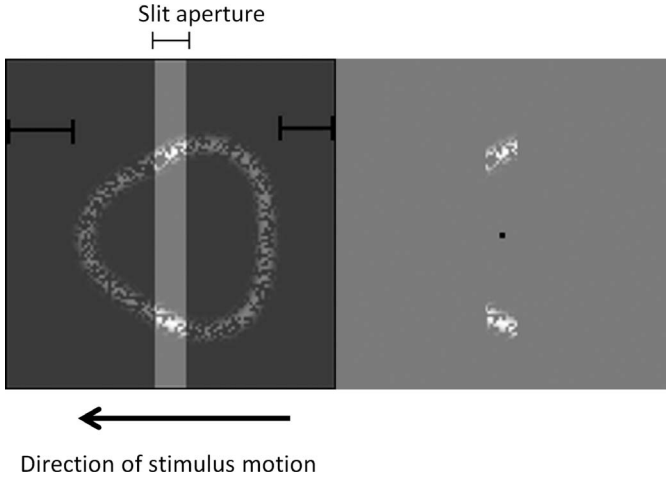

Figure 2. Example of moving pattern presentation, the stimulus is progressively revealed as it moves behind the slit; lower contrast sections were invisible but are shown for clarity (left). The stimulus as it appears to the observer (right). Note: The stimulus does not take up all of the stimulus window generated; therefore, when the slit is within the outer black brackets, only the fixation point is visible.

Multiscan G420 monitor (Sony Corp, Tokyo, Japan), with a frame rate of 100 Hz, from the frame buffer of a Cambridge Research Systems VSG 2/3 graphics card (CRS Ltd, Rochester, UK), housed in a PC with a 400 MHZ Pentium II processor (Intel, Santa Clara, CA). A Cambridge Research Systems OPTICAL OP 200-E photometer (CRS Ltd, Rochester, UK; head model number 265) performed the luminance calibration of the display. Background luminance was 45cd/m^2. The RF patterns had a maximum Weber contrast ($[L_{max} - L_{background}]/L_{background}$) of 1. Observer responses were made on a Cambridge Research Systems CB3 button box and a chin rest was used to set the viewing distance at 117.5 cm from the monitor, such that each screen pixel subtended 1′ of visual angle. The observer was instructed to fixate on a square static fixation point, with 4′ side length, which remained in the center of the screen during presentation of both intervals. The center of each pattern was able to vary ±6′ of visual angle in the horizontal and vertical directions.

Procedure

A two-interval forced choice (2IFC) procedure was used, consisting of a test stimulus (RF pattern) in one interval and a reference stimulus (circle; i.e., $A = 0$ in Equation 1) in the other. The order of presentation was randomized between trials and the observer chose which pattern appeared the most deformed from circular. Each interval consisted of 34 frames, with a frame duration of 40 ms and an interstimulus interval of 500 ms.

There were four conditions in Experiment 1: conventional presentation, the entire stimulus was visible to the observer; moving slit presentation, a slit moved over the stimulus progressively revealing it; moving pattern presentation, the pattern moved behind a stationary slit; and random slit presentation, a slit appeared at random locations revealing the stimulus in a piecemeal fashion. The slit used in all of the slit conditions was 10′ wide and extended above and below the stimulus boundary. In the moving slit and moving pattern conditions, the slit and the pattern (respectively) advanced in 3′ steps on each frame. The slit itself was implicit, with the slit boundary producing an illusory contour (see Figure 2), which observers reported appeared to extend above and below the upper and lower extent of the stimulus.

The stimulus window was larger than the absolute size of the stimulus, allowing the stimulus center to jitter randomly within a 6′ radius of the fixation point between trials and also allowing RF patterns of varying amplitudes. This extra space in the window (see black brackets in Figure 2) resulted in areas of the window that were purely background luminance (in other words, empty). This means that during the moving slit and moving pattern presentations, frames before and after the stimulus did not contain any contour information, therefore the stimulus did not occupy the full 34 frames in each trial. As the stimulus was 60′ in diameter and the slit 10′ wide (advancing in 3′ intervals), a stimulus with an infinitely small edge would occupy 24 frames in each interval, however, due to the Gaussian luminance profile the stimulus occupied 25 frames. This resulted in 1,000 ms presentation times for the moving slit, and moving pattern conditions and 1,360 ms presentation times for the conventional and random slit conditions. We do not believe this difference in presentation times between the conditions had an effect on the results since changing the stimulus presentation time did not have any effect on thresholds or integration strength (see Experiment 2).

Observer psychometric functions were sampled using the method of constant stimuli (MOCS), using nine amplitudes per block, three blocks per cycle of modulation, and three cycles of modulation per condition. Results were fitted using a Quick function:

$$p(A) = 1 - 2^{-\left[1+(A/\alpha)^{\beta}\right]} \quad (2)$$

where p is the probability of correct response, A is the amplitude of modulation as a proportion of the radius on an unmodulated circle, α is the threshold at the 75% correct response level and β controls the slope of the psychometric function. Thresholds were plotted against number of cycles and compared to probability summation predictions.

Previous studies have used high threshold theory (HTT) to provide an estimate of probability summation; however, evidence from Baldwin et al. (2016) has suggested this is an inappropriate method for RF patterns. We have included it here to provide a comparison with previous works. Probability summation predictions under HTT were estimated by $1/\bar{\beta}$, where $\bar{\beta}$ is the average of the slopes of the psychometric functions for all cycles of the RF pattern.

As an alternative to HTT, signal detection theory (SDT) has been used in recent publications to generate probability summation estimates. This was done by estimating d prime (d') using:

$$d' = (gA)^{\tau} \quad (3)$$

where d' is internal strength of a signal, g is a scaling factor incorporating the reciprocal of the internal noise standard deviation, A is the stimulus intensity, and τ is the exponent of the internal transducer (rate at which observer is converting increased stimulus intensity to increased perception). Under SDT the estimated percentage correct for probability summation was given by (Kingdom, Baldwin, & Schmidtmann, 2015):

$$\mathrm{Pc} = n \int_{-\infty}^{\infty} \phi(t-d')\Phi(t)^{QM-n}\Phi(t-d')^{n-1}dt + (Q-n)\int_{-\infty}^{\infty} \phi(t)\Phi(t)^{QM-n-1}\Phi(t-d')^{n}dt \quad (4)$$

where Pc is the percentage correct and set at 75%, t is sample stimulus strength, the heights of the noise and signal distributions at t are given by $\phi(t)$ and $\phi(t-d')$ respectively, $\Phi(t)$ and $\Phi(t-d')$ are the areas under the noise and signal distributions below stimulus strength t, Q is the number of monitored channels, M is the number of alternatives in the forced choice task, and n is the number of stimulus components. This equation is implemented in the Palamedes toolbox (Prins & Kingdom, 2009, available at http://www.palamedestoolbox.org).

The number of channels included (Q) in estimates of probability summation under SDT have a large effect on the resulting predicted strength of integration. Previous research by Cribb, Badcock, Maybery, and Badcock (2016) has used both a "low" and "high" number of channels to provide an ultra-conservative estimate (low number of channels; $Q = 3$; and consistent with Baldwin et al., 2016) and a more theoretically appropriate estimate (high number of channels; $Q = 120$). The same method will be employed by the current study.

Results

Figure 3 displays the thresholds for all five observers along with the averaged thresholds across the five observers for each condition. A repeated-measures 4 (conventional, moving pattern, moving slit, random) × 3 (one cycle, two cycles, three cycles) factorial analysis of variance (ANOVA) was used to examine the effect of condition and the number of cycles of modulation on observer thresholds. There was a significant main effect of cycles of modulation, $F(2, 8) = 43.72$, $p < 0.001$, $\eta_p^2 = 0.92$, and there was also a significant interaction effect, $F(6, 24) = 15.65$, $p < 0.001$, $\eta_p^2 = 0.80$. Mauchly's test of sphericity was violated for Condition, so Greenhouse–Geisser correction was applied, $F(1.24, 4.95) = 88.61$, $p < 0.001$, $\eta_p^2 = 0.96$. Bonferroni-adjusted pairwise comparisons revealed a significant difference between all cycles of modulation (all ps < 0.05), with thresholds for one cycle larger than both two, and three cycles and two-cycle thresholds larger than three cycles. Bonferroni-adjusted pairwise comparisons also revealed there was no significant difference between the moving pattern and moving slit conditions ($p > 0.05$); however, there was a significant difference between all other pairwise comparisons between the conditions (ps < 0.05). As can be seen in the caption of Figure 3, the slope of the conventional condition (black dots with black line) is steeper than the other three conditions, driving the significant interaction effect.

A repeated-measures 4 (observed, HTT PS, SDT 3 channels PS, SDT 120 channels PS) × 4 (conventional, moving pattern, moving slit, random) factorial ANOVA was used to examine the effects of the different slope estimates and condition on the strength of integration. There was no significant main effect of condition, $F(3, 12) = 1.77$, $p = 0.20$, $\eta_p^2 = 0.31$, and there was no significant interaction effect, $F(9, 36) = 0.37$, $p = 0.94$, $\eta_p^2 = 0.09$. There was a significant main effect of type of slope, $F(3, 12) = 64.48$, $p < 0.001$, $\eta_p^2 = 0.94$. Planned comparisons found observer slopes were significantly steeper than probability summation slope estimates by HTT and SDT, for both low and high number of channels (all ps < 0.01). Figure 4 displays the mean observer slopes, and the mean probability summation slopes under HTT and SDT.

SDT predicts that stimuli for which thresholds are determined by probability summation will exhibit a decrease in psychometric slope with increasing number of local elements (Kingdom et al., 2015; Pelli, 1985). Figure 5 displays the mean psychometric slopes for all four conditions. There appears to be no decrease in psychometric slopes with increasing numbers of cycles of modulation for any of the conditions. No significant linear trends were found for any of the conditions: conventional, $F(1, 4) = 0.03$, $p = 0.87$, $\eta_p^2 = 0.01$; moving pattern, $F(1, 4) = 0.08$, $p = 0.79$, $\eta_p^2 = 0.02$; moving slit,

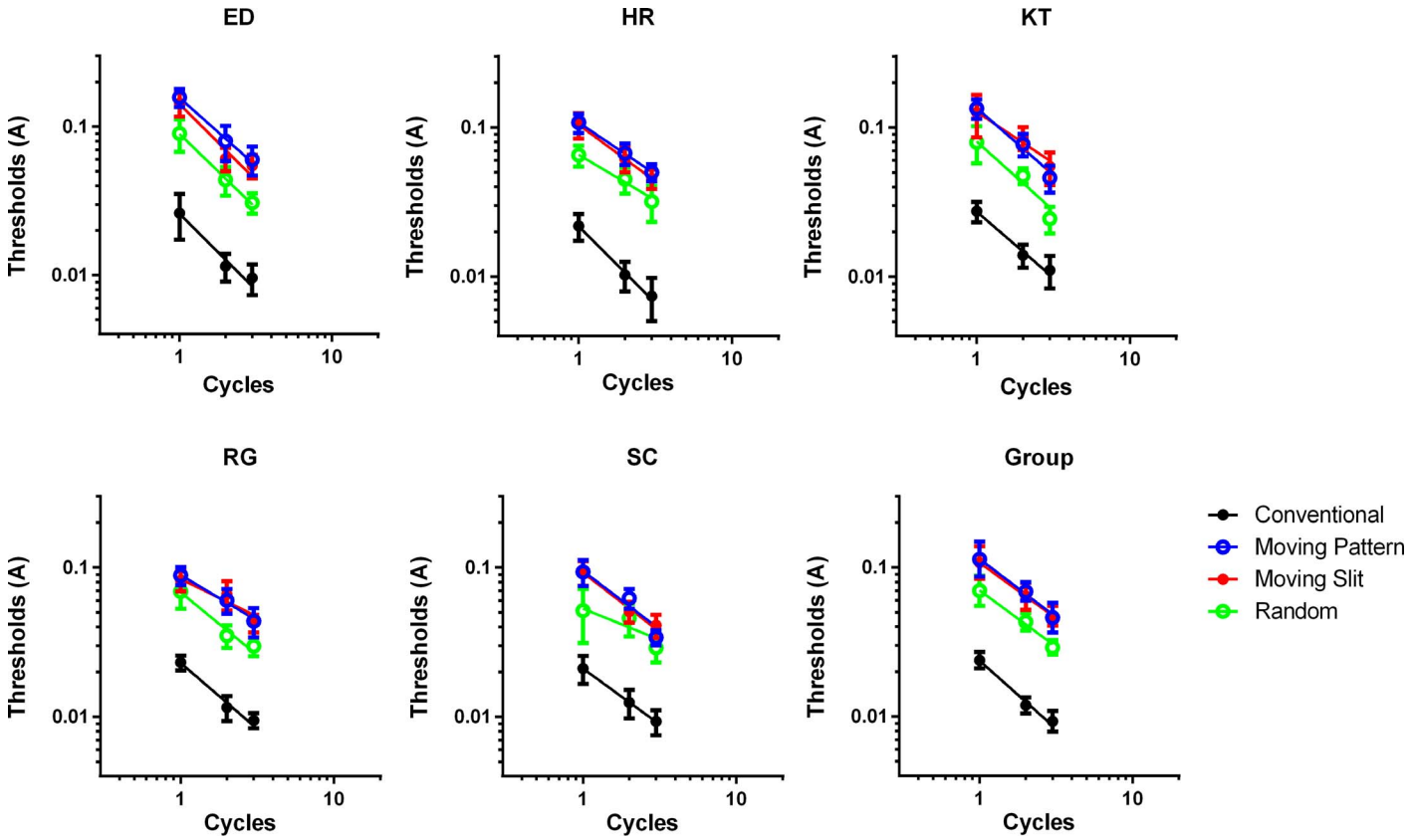

Figure 3. Thresholds with 95% confidence intervals for each observer, along with the geometric mean for all observers (group) for: conventional condition (black circle; −0.92); moving pattern (blue open circle; −0.78); moving slit (red circle; −0.75); and random (green open circle; −0.76).

$F(1, 4) = 3.18$, $p = 0.15$, $\eta_p^2 = 0.44$; and random slit, $F(1, 4) = 2.70$, $p = 0.18$, $\eta_p^2 = 0.40$. Although there is variation in the data, our results are consistent with Baldwin et al. (2016) and with other work from our lab, which suggests no change in psychometric slopes with an increase in the number of cycles of modulation.

Summary

There was no difference between the thresholds of the moving pattern condition and the moving slit condition. Viewing an RF pattern under either of these conditions resulted in thresholds approximately four times greater than under conventional viewing conditions (i.e., a static, freely visible, contour-defined pattern). The random condition had thresholds slightly lower than the moving slit/moving pattern conditions but was still approximately three times greater than under conventional viewing conditions.

Despite the difference in thresholds, there was no difference in the strength of integration between any of the conditions. In other words although there was a difference in the observers' sensitivities to contour information for some of the conditions, it did not affect their ability to combine that information around the contour. There was also evidence of global processing for all conditions under both HTT and SDT (for a high and low number of channels), and there was no evidence for a decrease in psychometric slope with increasing numbers of cycles of modulation.

Experiment 2

The visual system combines information over time to enhance sensitivity. Legge (1978) showed that contrast sensitivity measured using both "low" spatial frequency (<1.5 c/deg) and "high" spatial frequency (>1.5 c/deg) targets increased until the presentation time reached either 100 ms for low or 1,000 ms for high spatial frequency, after which it asymptotes. Evidence for integration windows has also been shown for visual acuity using Landolt rings up to 400 ms (Baron & Westheimer, 1973) and global motion using dynamic Glass patterns up to 3,000 ms (Burr & Santoro, 2001; Ross, Badcock, & Hayes, 2000).

Given the visual system is thought to be a hierarchy of visual processing stages, pooling information from lower

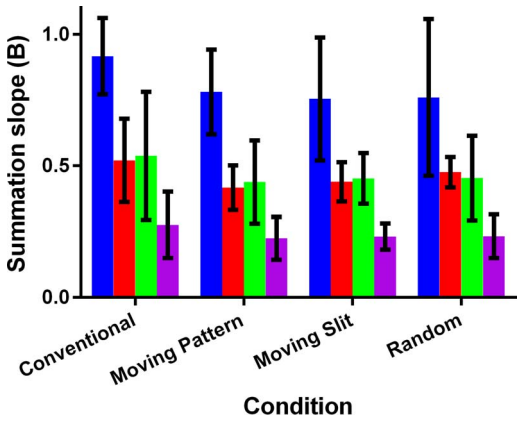

Figure 4. Results averaged across five observers with 95% confidence intervals. Observer slopes (blue) and probability summation slope estimates under HTT (red), SDT using a low number of channels (green), and SDT using a high number of channels (purple).

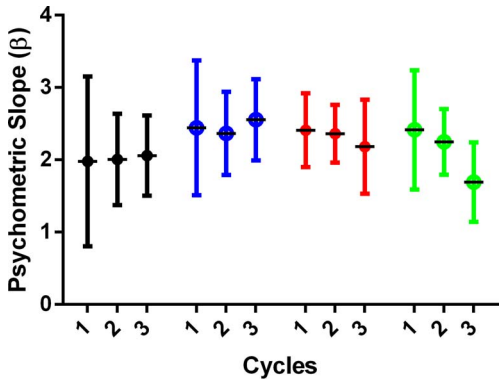

Figure 5. Psychometric slopes for all conditions with 95% confidence intervals: conventional (black circle); moving pattern (blue open circle); moving slit (red circle); and random slit (green open circle).

levels of the visual pathway (Felleman & Van Essen, 1991; Van Essen, Anderson, & Felleman, 1992), we may expect that global integration of contour information also has a temporal limit, with all of the shape information needing to be presented within a specific time frame. Research presented by Bell, Sacks, and Burr (2015) suggested that there was no effect of presentation time (measured from 10–320 ms) on integration, but they did find that sensitivity improved with increased presentation time. Our results from Experiment 1 demonstrate strong evidence for global processing for presentation times up to 1,360 ms. Therefore, for Experiment 2, we wanted to determine if, similar to Bell et al. (2015), changes in presentation time would result in changes in observer thresholds (sensitivity) and if our comparatively longer presentation times (4,000 ms compared to the 320 ms in Bell et al., 2015) were able to effect the integration of information around the contour.

Methods

The same observers, apparatus, stimuli and procedure from Experiment 1 were used in Experiment 2; however, only the moving slit condition (stationary RF pattern of random phase, progressively revealed by a moving implicit slit) was tested with five different presentation times. As outlined already there were 34 frames presented; however, only 25 contained stimulus information. For Experiment 2 the duration of each frame for the respective conditions were: 10 ms; 20 ms; 40 ms; 80 ms; and 160 ms. This resulted in presentation times of 250, 500, 1,000, 2,000, and 4,000 ms per interval.

Results

Figure 6 shows the mean thresholds (five observers) for each of the five conditions and all five conditions together. A repeated-measures 5 (250, 500, 1,000, 2,000, 4,000) × 3 (one cycle, two cycles, three cycles) factorial ANOVA was used to examine the effect of presentation time and number of cycles on observer thresholds. There was a significant main effect of number of cycles, $F(2, 8) = 57.70$, $p < 0.001$, $\eta_p^2 = 0.94$, but there was no significant effect of presentation time, $F(4, 16) = 1.44$, $p = 0.27$, $\eta_p^2 = 0.27$, and there was no interaction effect, $F(8, 32) = 0.72$, $p = 0.67$, $\eta_p^2 = 0.15$. Pairwise comparisons revealed that thresholds for one cycle was significantly greater than two, and three cycles and thresholds for two cycles was significantly greater than three cycles.

A repeated-measures one-way ANOVA was used to compare observer slopes with the slopes from the three probability summation estimates. There was a significant main effect for all conditions: 250, $F(3, 12) = 15.00$, $p < 0.001$, $\eta_p^2 = 0.79$; 500, $F(3, 12) = 17.38$, $p < 0.001$, $\eta_p^2 = 0.81$; 1,000, $F(3, 12) = 19.87$, $p < 0.001$, $\eta_p^2 = 0.83$; 2,000, $F(3, 12) = 37.71$, $p < 0.001$, $\eta_p^2 = 0.90$; and 4,000, $F(3, 12) = 37.62$, $p < 0.001$, $\eta_p^2 = 0.90$. Planned comparisons revealed no significant difference between observer slopes and SDT three-channels probability summation estimates for the 250 ms and 500 ms presentation times ($ps > 0.05$). All other comparisons showed a significant difference between observer slopes and their respective probability summation estimates ($ps < 0.05$).

Figure 7 displays the mean sensitivity (at one cycle of modulation) and integration slopes for the five observers. A repeated-measures one-way ANOVA was used to examine the effect of presentation time on sensitivity. There was no significant main effect of presentation time, $F(4, 16) = 0.81$, $p = 0.54$, $\eta_p^2 = 0.17$ and there was no significant linear trend, $F(1, 4) = 0.03$,

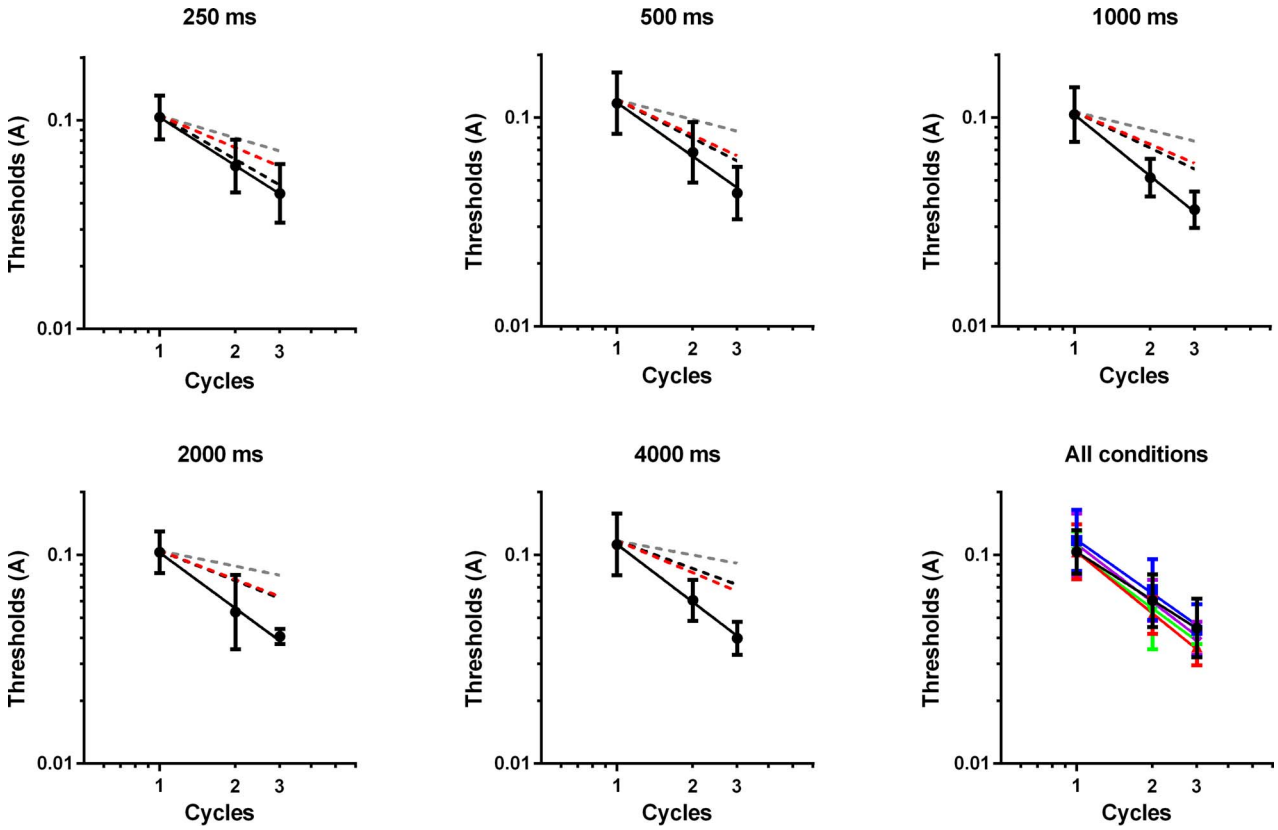

Figure 6. Results for moving slit condition with increasing presentation durations and individual data. Thresholds are the geometric means for five observers with 95% confidence intervals, observer slopes (solid black line), and probability summation estimates: HTT (red dashed); SDT three channels (black dashed); and SDT 120 channels (gray dashed). Lines of best fit for all slopes were $R^2 > 0.99$, with values of: −0.75 (250 ms); −0.86 (500 ms); −0.99 (1,000 ms); −0.88 (2,000 ms); and −0.95 (4,000 ms). The grouped graph displays all 5 conditions: 250 ms (black); 500 ms (blue); 1,000 ms (red); 2,000 ms (green); and 4,000 ms (purple).

$p = 0.88$, $\eta_p^2 = 0.01$. Another repeated measures one-way ANOVA was used to examine the effect of presentation time on observer slopes and indicated no significant main effect of presentation time, $F(4, 16) = 1.02$, $p = 0.43$, $\eta_p^2 = 0.20$, and there was also no significant linear trend, $F(1, 4) = 1.97$, $p = 0.23$, $\eta_p^2 = 0.33$.

Summary

There was no effect of presentation time on observer thresholds nor strength of integration. There was strong evidence of global processing for the 1,000, 2,000, and 4,000 ms conditions, with observer slopes

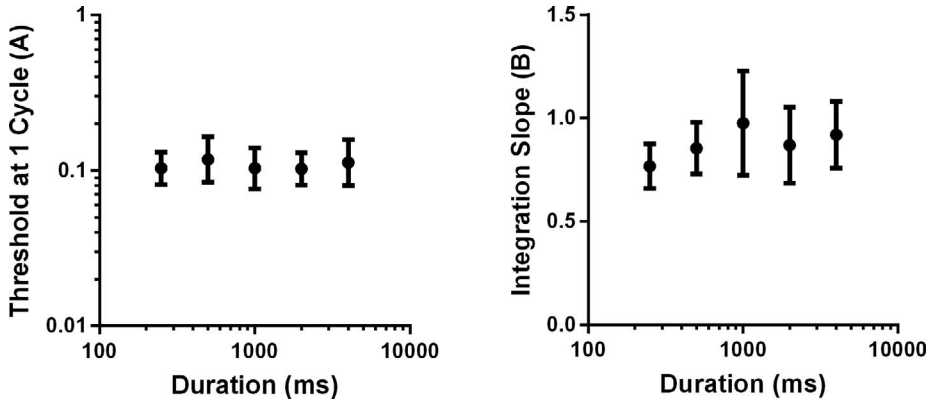

Figure 7. Geometric mean with 95% confidence intervals of the threshold at one cycle of modulation (left) and mean integration slopes with 95% confidence intervals (right) for five observers. There appears to be no effect of presentation time (duration) on strength of integration or sensitivity

significantly steeper than all probability summation estimates. For the 250 and 500 ms conditions observer slopes were steeper than both HTT and SDT for an appropriate number of channels (120 channels), but not significantly steeper than the extremely conservative SDT probability summation slope (three channels) in which observers would be required to know where the deformation would occur (fixed phase). Therefore, we also interpret the data for the 250 and 500 ms conditions as evidence of global processing. Similar to Bell et al. (2015), we found no effect of presentation time on integration slopes; however, we found no changes in sensitivity (see below for further discussion). Logically, there must be a limit to which the visual system can integrate information around a shape's contour; however, we have no indication from our data what that limit might be as there appeared to be no trend apparent and further investigation is required.

Experiment 3

As mentioned already, Or et al. (2011) used a difference of Gaussian (DOG) dot to trace out the path of an RF pattern over a period of 1 and 2 s (Figure 8). They found evidence for global integration of this motion RF pattern, with improvement in detection of trajectory modulation approximating a power function with a slope of −0.64. This result is not typical of static RF3 patterns, however, where slopes are generally steeper: −0.86 (Loffler et al., 2003); −0.75 (Almeida, Dickinson, Maybery, Badcock, & Badcock, 2010); and −0.92 (Tan et al., 2013).

Or et al. (2011) suggested the relatively shallow (for an RF3) integration slope was a result of the difficulty of the task, with presentation times of 1 and 2 s requiring the use of memory, which in turn results in extra processing and, therefore, poorer integration. However, given our results in Experiment 2 demonstrated quite steep integration slopes at comparable durations (−0.99 for 1,000 ms; −0.88 for 2,000 ms; and −0.95 for 4,000 ms) and had probability summation estimates under both HTT and SDT (three channels) which were around −0.60, we decided to reexamine the results of Or et al. (2011) to determine if global processing was occurring for these patterns, why the integration around these patterns is comparatively poor, and whether there is any evidence for form processing of these stimuli.

One explanation for the decreased strength of integration is possibly the use of constant angular speed by Or et al. (2011). A dot tracing an RF pattern with constant angular velocity will have changes in retinal speed to allow for variations in the radius. This change

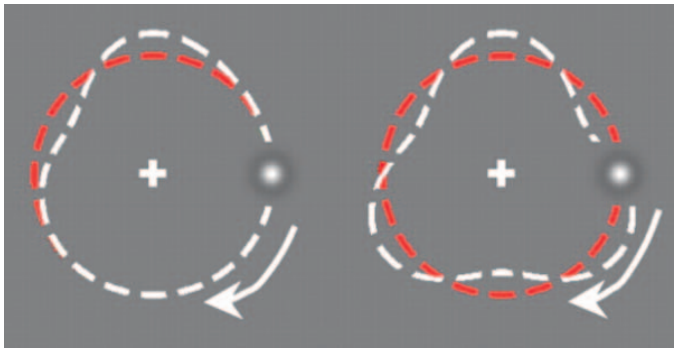

Figure 8. Motion RF patterns (from Or et al., 2011): RF3 with one cycle of modulation (left); RF3 with three cycles of modulation (right). White dashed line indicates the path taken by the dot tracing the test stimulus (motion RF), and the red dashed line shows the path traced by the reference stimulus (a circle, i.e., $A = 0$ in Equation 5).

in retinal speed could result in a local cue, which is preferentially used at low numbers of cycles where the global signal is relatively weak. As each cycle is added to the pattern the global shape signal increases and can eventually become more salient than the local cue (see experiment 3 in Dickinson et al., 2012). This interaction between local and global signal would reduce thresholds for lower numbers of cycles selectively and thus give the result of a relatively shallow integration slope and potentially describe the results obtained by Or et al. (2011).

Or et al. (2011) did anticipate the possibility of this speed cue and examined observer thresholds as a function of radial frequency for patterns with constant angular velocity and constant retinal speed. They concluded there was no effect of the constant angular velocity, as there was no significant difference between the slopes nor y-intercepts of the fitted functions relating radial frequency to threshold for detection. However, this was done with complete RF patterns (i.e., RF patterns with all cycles of modulation present) and would likely have a strong global signal from the pattern. Therefore, they were likely correct in their conclusion that angular velocity does not have an effect on complete RF patterns, but they did not test the effect of angular velocity on incomplete patterns.

One of the main reasons for creating this motion RF stimulus was to analyse periodic motion with a view to assessing its contribution to the perception of biological motion (Or et al., 2011). Thus, Or et al. (2011) suggested these stimuli were processed in motion regions of the brain. Gorbet, Wilkinson, and Wilson (2012) and Gorbet, Wilkinson, and Wilson (2014), using fMRI, suggested their data supported the view that these patterns are processed in motion regions of the brain, however, they were unable to rule out the possibility that motion RFs were actually being

processed as form information due to temporal integration of motion streaks.

The temporal integration of single neurons in V1 can result in object motion producing visual streaks of oriented information and this has been shown to aid the visual system in determining motion direction (Badcock & Dickinson, 2009; Geisler, 1999; Ross et al., 2000; Tang, Dickinson, Visser, & Badcock, 2015). Research has suggested this information is not only coded in V1 (Apthorp et al., 2013), but at multiple levels up to STS (Mather, Pavan, Bellacosa Marotti, Campana, & Casco, 2013) and that a considerable number of connections occur between the dorsal and ventral streams of the visual system (Takemura et al., 2016). Therefore, it is possible that these motion RF patterns are being processed within the ventral visual stream similar to static, contour-defined RF patterns.

Previous behavioural studies support this hypothesis as the processing of motion RF patterns (Daar, Or, & Wilson, 2012; Or et al., 2011; Wilkinson, Haque, Or, Gottlieb, & Wilson, 2016; Wilson & Fung, 2016) show a similar pattern of results compared to static RF patterns when changing parameters such as radius, frequency, and cycles of modulation (Bell, Wilkinson, Wilson, Loffler, & Badcock, 2009; Loffler et al., 2003; Wilkinson et al., 1998). Furthermore, Gorbet et al. (2012) compared the results of motion RF patterns with those obtained with open motion patterns (a sinusoidally modulated line pattern revealed by a dot with a DOG profile, tracing either two or three cycles). They found there was no difference in the activation of areas MT and STS when comparing motion RF patterns to these motion-defined modulated lines. We believe this lack of increased activation in motion areas during the motion RF condition is evidence that motion information is not being integrated within this region, but is instead being combined in the form regions.

Therefore, Experiment 3 will replicate the experiment of Or et al. (2011) using constant angular velocity and also test the effect of constant retinal speed on observer thresholds but with a set of patterns that will allow the measurement of the complete integration function. We predict that fixed angular velocity will produce reduced observer thresholds for incomplete patterns, but not complete patterns, because of the salient local cue provided by the retinal speed changes, reducing observer thresholds for these incomplete patterns. Following on from the open motion patterns (sinusoidally modulated lines traced out by a DOG dot) created by Gorbet et al. (2012) we will also compare observer thresholds of contour-defined modulated lines (sinusoidally modulated lines analogous to an uncoiled RF pattern; see Figure 9) with motion-defined modulated lines and predict that, similar to the results of the motion-defined and contour-defined RF patterns, these stimuli will also demonstrate the same pattern of results.

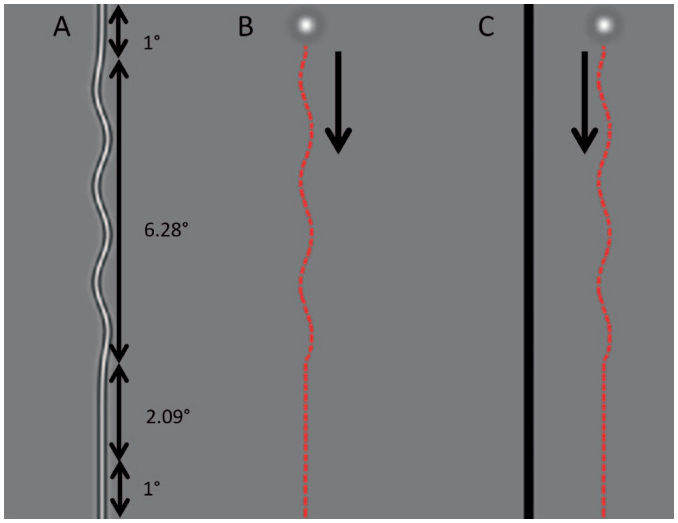

Figure 9. Dimensions of the line stimuli used: (A) contour line; (B) motion line; (C) motion line fixation.

Methods

Observers

The two authors who participated in Experiments 1 and 2 and two naïve observers participated in the current experiment, all with normal or corrected-to-normal visual acuity, which was assessed using a LogMAR chart. Informed written consent was given and conformed to both University of Western Australia ethics committee and the Declaration of Helsinki.

Stimuli

In this experiment a dot traced out an RF pattern over time (t), at angular speed (v), as defined by Or et al. (2011):

$$r(vt) = r_0 \times [1 + A\sin(\omega vt + \varphi)] \quad (5)$$

where r is the dot's polar location, r_0 is the mean radius (1° of visual angle in all conditions to maintain consistency with Or et al., 2011), A is the amplitude of modulation (proportion of mean radius), ω is the frequency of modulation (number of cycles per 2π radians) and φ is the phase of the sinusoidal modulation. Another way to define this equation, so as to include polar angle into the function would be:

$$r[\theta(t)] = r_0 \times \{1 + A\sin[\omega\theta(t) + \varphi]\} \quad (6)$$

where the parameters are the same as for Equation 5 and $\theta(t) = 2\pi t/[F_r(F_n - 1)]$, with F_r being the frame duration in ms, F_n is the total number of frames to display, and t is time in ms. The dot used was a

difference of Gaussians (DOG), again identical to that used by Or et al. (2011):

$$\mathrm{DOG}(R) = 1.8\exp\left(-R^2/\sigma^2\right) - 0.8\exp\left[-R^2/(1.5\sigma)^2\right] \quad (7)$$

where R is the radius of the DOG and σ was set to 7.1′ of visual angle. As in Or et al. (2011), the pattern is spread over several pixels with varying intensity allowing subpixel precision in the dot's spatial position.

In addition to the motion RF stimuli, line stimuli were also employed to see if the closed contour was critical to the outcome. The length of the modulated sector for all line stimuli was 6.28° of visual angle (the equivalent length of an uncoiled RF pattern with a 1° radius), with an additional 2.09° of visual angle (the equivalent length of one cycle of modulation) in which the modulated sector could begin (i.e., the starting location of the modulation varied randomly between trials), and another 1° of visual angle at the top and bottom of the lines to avoid positional cues between the line ends and the start of modulation (see Figure 9).

There were three line conditions: motion line; motion line fixation; and contour line. The purpose of the motion line conditions is to determine if, similar to the contour-defined results found by Green et al. (2017), open motion patterns are processed in a different way to the closed contour motion RF patterns. The motion line and motion line fixation conditions consist of a DOG dot (as defined in Equation 7) tracing out the path of a modulated line which was either by itself (motion line) or 1° of visual angle to the side of a solid black line (motion line fixation; the same distance as between the fixation point and the dot used for the motion RF patterns). The motion line fixation condition was created to enable the observer to use the fixation to aid in their judgement of the dot's horizontal motion. This was designed to be analogous to the observer tracking the dot with their eyes in the motion RF conditions and using the fixation square to judge its change in radius and so observers were instructed to follow the dot's motion with their eyes.

For the contour line condition and similar to conventional RF patterns (Loffler et al., 2003) and previous contour-defined modulated lines (Green et al., 2017), the cross section of the luminance profile of the path conformed to a fourth derivative of a Gaussian (D4) with a frequency spectrum peaking at 8 c/deg where $f_{\mathrm{peak}} = \sqrt{2}/\pi\sigma$ (Loffler et al., 2003; Wilkinson et al., 1998) and obtained using a σ of 3.376′ of visual angle.

Apparatus

Stimuli were generated using a PC (Pentium 4, 2.4 GHz) and custom software written in MATLAB 7.2.0 (MathWorks). The observers viewed a CRT Sony Trinitron CPD-G420 monitor (100 Hz refresh rate), which presented the stimuli from the frame buffer of a Cambridge Research Systems (CRS) VSG2/5 visual stimulus generator. Screen resolution was 1,024 × 768 pixels and viewing distance was stabilized at 58.75 cm using a chinrest, which resulted in each pixel subtending a visual angle of 2′. An Optical Op200-e photometer (head model number 265) was used to linearize the luminance response and to calibrate background luminance to 45 cd/m^2 and maximum luminance to 90 cd/m^2, resulting in a Weber contrast of 1. Responses were signaled using the left and right buttons of a mouse. A square fixation point (6′ side length) was used to indicate the center of the screen where stimuli were presented.

Procedure

For the motion RF stimuli, a two-interval-forced-choice (2IFC) paradigm was used for both conditions, with observers reporting which interval contained a dot tracing out the pattern, which was most deformed from a circular path. One interval contained the reference stimulus, which consisted of a dot tracing out a circle ($A = 0$ in Equation 1). The other interval contained the test stimulus, with a dot tracing out a circle with one, two, or three cycles of RF3 modulation. Order of presentation was randomized between trials. Each stimulus was presented for 1,000 ms, with a 500 ms interstimulus interval. There were twenty-five 40-ms frames, with the first and last frames identical to each other (resulting in the dot finishing at its starting location). Each condition was tested in three blocks, one for each cycle of modulation (i.e., one, two, and three cycles) and these were randomized for each participant. For the *angular velocity* condition, the dot traced out a random phase pattern with a constant angular velocity (6.28°/s), meaning the dot appeared every $\pi/12$ radians, starting and finishing at the 3 o'clock position (see Figure 8). For the *retinal speed* condition, the total path length was calculated and the dot then moved 1/24 of the distance of the path each frame (again the phase of the pattern was random). As can be seen in Figure 10, the two conditions produce almost identical differences in radii (peak and trough) and have the greatest difference in dot locations occurring around the zero crossing of the modulation function (180° in figure).

Observers were instructed to follow the dot with their eyes for the motion line fixation condition, but for the contour line and motion line conditions there was no fixation point, so observers were able to freely view the stimulus. Again, a 2IFC paradigm was used for all conditions, with observers reporting which interval contained a modulated line (contour line condition) or

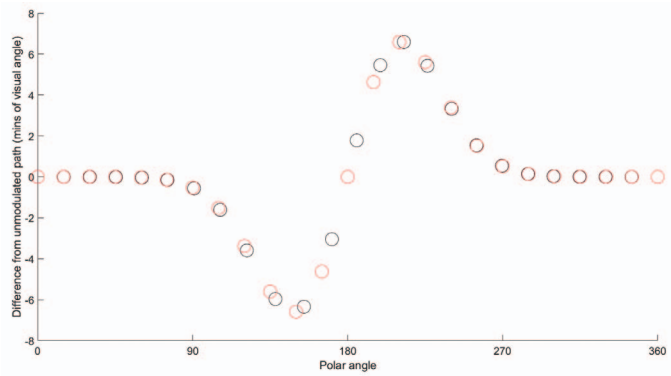

Figure 10. Polar location of dot for constant angular velocity (red) and constant retinal speed (black) with the same amplitude (approximately threshold level) for an RF3(1). *Y*-axis displays the radial location in minutes of visual angle in relation to an unmodulated pattern ($A = 0$ in Equation 5).

a dot which has traced the path of a modulated line (motion line and motion line fixation conditions). To reduce total number of trials and participant fatigue, data was collected using the PSI method (Kontsevich & Tyler, 1999), implemented using the Palamedes toolbox (Prins & Kingdom, 2009, downloaded 2015 from http://www.palamedestoolbox.org), which optimized a Quick function (Quick, 1974; see Equation 2). One hundred and fifty trials were performed for each cycle of modulation for each condition.

Results

To examine the effect of condition and number of cycles on observer thresholds for an RF3 a repeated-measures 2 (retinal speed, angular velocity) × 3 (one cycle, two cycles, three cycles) factorial analysis of variance (ANOVA) was used. There was a significant main effect of condition, $F(1, 3) = 67.92$, $p = 0.004$, $\eta_p^2 = 0.96$, and a significant main effect of number of cycles, $F(2, 6) = 63.66$, $p = 0.004$, $\eta_p^2 = 0.96$. The interaction violated the assumption of sphericity and there was no significant interaction effect after Greenhouse–Geisser adjustment was applied, $F(1, 3) = 9.09$, $p = 0.06$, $\eta_p^2 = 0.75$. Pairwise comparisons indicated a significant difference between all cycles of modulation (all ps < 0.05), with one cycle of modulation having the highest threshold and three cycles having the lowest. Table 1 displays the descriptive statistics along with paired sample t tests comparing each condition at each number of cycles of modulation. A paired samples t test found retinal speed slopes ($M = 0.80$, $SD = 0.11$) were, on average, significantly steeper than angular velocity slopes ($M = 0.70$, $SD = 0.14$), $t(3) = 3.64$, $p = 0.04$, $d = 1.82$. Although there appears to be slightly more variation at one cycle of modulation compared to two and three cycles, repeating the ANOVA using log transformed data did not yield different results.

	Retinal speed		Angular velocity			
	M	*SD*	*M*	*SD*	*p* value	Cohen's *d*
1 Cycle	0.121	0.026	0.100	0.025	0.001*	6.35
2 Cycles	0.078	0.019	0.065	0.022	0.03*	2.07
3 Cycles	0.045	0.017	0.046	0.014	0.95	0.03

Table 1. Descriptive statistics for retinal speed and angular velocity conditions at one, two, and three cycles of modulation along with significance values and Cohen's *d* scores from paired samples *t* tests comparing the two conditions at the corresponding numbers of cycles of modulation. *Notes*: *$p < 0.05$.

Figure 11 displays the ratio of observer thresholds for the constant angular velocity and constant retinal speed conditions. A linear regression of the data ($R^2 = 0.94$; slope = 0.79, CI [0.65, 0.93]) is significantly shallower than a slope of 1, $F(1, 10) = 11.77$, $p = 0.007$. This data clearly shows what is described in Table 1, observers at one cycle of modulation are comparatively poor (below the dashed line) at the retinal speed condition compared to the angular velocity condition. This difference is reduced at two cycles and is absent for three cycles of modulation.

To examine global processing, a one-way repeated-measures ANOVA was used to determine the difference between the measured slope and those predicted by probability summation under HTT and SDT. For the angular velocity, there was a significant main effect of slopes (angular velocity, HTT PS, SDT 3 channels PS, SDT 120 channels PS), $F(3, 9) = 11.23$, $p = 0.002$, $\eta_p^2 = 0.79$. Planned comparisons revealed no significant difference between the angular velocity slope and those predicted by probability summation for all models and number of channels (all ps > 0.05). Pairwise comparisons revealed the significant difference was a result of the difference between the two SDT probability summation estimates ($p < 0.05$). For retinal speed, there was a significant main effect of slopes (retinal speed, HTT PS, SDT 3 channels PS, SDT 120 channels PS), $F(3, 9) = 12.22$, $p = 0.002$, $\eta_p^2 = 0.80$. Planned comparisons revealed a significant difference between retinal speed slope and all of its probability summation estimates for all models and number of channels (all ps < 0.05).

Figure 12 displays the results averaged across four observers for the contour-defined and motion-defined modulated lines. A repeated-measures 3 (contour line, motion line, motion line fixation) × 3 (one cycle, two cycles, three cycles) factorial ANOVA was used to investigate the effect of conditions and number of cycles on observer thresholds. There was a significant main effect of both condition, $F(2, 6) = 10.87$, $p = 0.01$, $\eta_p^2 = 0.78$, and number of cycles, $F(2, 6) = 25.63$, $p =$

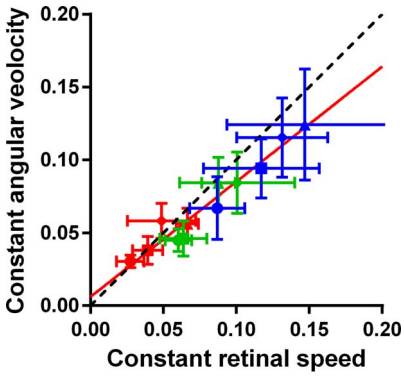

Figure 11. Plot of the ratio of observer thresholds with each observer as a different shape and their respective 95% confidence intervals. Colored data points correspond to: one cycle (blue); two cycles (green); and three cycles (red). Red solid line represents a linear regression of the ratios ($R^2 = 0.94$), whereas the black dashed line represents a line with the function $y = x$.

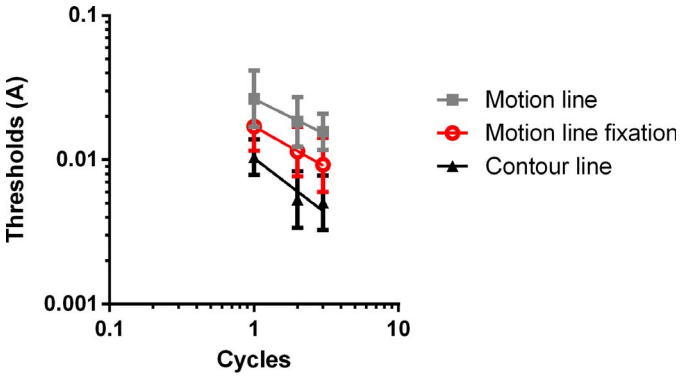

Figure 12. Geometric means of the four participants with 95% confidence intervals. The gray squares (top) show the motion line condition (−0.50), the red open circles (middle) show the motion line fixation condition (−0.57), and the black triangles (bottom) show the contour line condition (−0.77).

0.001, $\eta_p^2 = 0.90$. There was no significant interaction effect, $F(4, 12) = 1.89$, $p = 0.18$, $\eta_p^2 = 0.39$. Bonferroni-adjusted pairwise comparisons found no significant difference between any of the conditions ($ps > 0.05$) and a significant difference between both one and two cycles and one and three cycles ($ps < 0.05$), but no significant difference between two and three cycles of modulation ($p > 0.05$).

To compare observer slopes (strength of integration) and the slopes of probability summation estimates a 3 (contour line, motion line, motion line fixation) × 4 (observer slope, HTT PS, SDT 3 channels PS, SDT 120 channels PS) repeated-measures ANOVA was performed. There was no significant main effect of condition, $F(2, 6) = 1.51$, $p = 0.29$, $\eta_p^2 = 0.34$, nor probability summation estimate, $F(3, 9) = 3.42$, $p = 0.06$, $\eta_p^2 = 0.53$. There was also no significant interaction effect, $F(6, 18) = 1.09$, $p = 0.41$, $\eta_p^2 = 0.27$.

Only two of the observers from Experiment 1 participated in Experiment 3, so to compare observer thresholds between the moving slit, moving pattern, and constant retinal speed conditions, a 3 (one cycle, two cycles, three cycles; within groups) × 3 (moving slit, moving pattern, retinal speed; between groups) mixed-design ANOVA was used. There was a significant within subjects effect of cycles of modulation, $F(2, 22) = 116.32$, $p < 0.001$, $\eta_p^2 = 0.91$, but no significant between subjects effect of condition, $F(2, 11) = 0.25$, $p = 0.79$, $\eta_p^2 = 0.04$. There was also no interaction effect, $F(4, 22) = 0.55$, $p = 0.70$, $\eta_p^2 = 0.09$. Pairwise comparisons indicated a significant difference between all cycles of modulation (all $ps < 0.001$) with thresholds at one cycle of modulation the highest and three cycles of modulation the lowest.

Summary

The results show that the angular velocity stimulus had significantly lower detection thresholds than the retinal speed stimulus at both one and two cycles of modulation. There was no difference at three cycles of modulation. The retinal speed stimulus had a significantly steeper integration slope than the angular velocity stimulus and there was also evidence of global processing of the retinal speed stimulus, but no evidence of global processing for the angular velocity stimulus. These results are consistent with the interaction between a salient local cue and global signal.

For the line stimuli, there was no significant difference in either thresholds (after Bonferroni correction) or strength of integration for any of the conditions. Thresholds decreased only when moving from one to two cycles of modulation, but not between two and three cycles of modulation. There was also no evidence of global processing in any of the three conditions. Both the pattern of results and the comparison to probability summation estimates suggest that motion RF patterns are processed differently to motion line patterns. These findings support that of Green et al. (2017), but are contrary to those of (Schmidtmann & Kingdom, 2017) and are discussed as follows.

There was no significant difference in the observer thresholds for the moving slit, moving pattern, and retinal speed conditions. This suggests that it does not matter whether the shape of an RF pattern is revealed by a dot tracing its path or a slit progressively revealing its contour, an RF pattern presented over time results in the same observer thresholds within the limits tested here.

General discussion

The results of the current study have been quite surprising. It appears to indicate that although presenting an RF pattern over time (whether through a slit or traced by a dot) decreases observer sensitivity, it does not significantly affect the strength of integration of information around the contour. Changing the duration of presentation also appears to have no effect on an observer's ability to combine this information together.

For Experiment 1 we examined the effect of slit presentation of an RF pattern. For the moving slit condition (where a slit progressively reveals a stationary RF pattern) it could be argued integration over a 1 s presentation time could still be accounted for by low level effects. Perhaps visual aftereffects made the information available for enough time after the slit had moved past to facilitate integration. This kind of argument, however, cannot account for the moving pattern condition (where an RF pattern moves behind a stationary slit), as all of the information falls on the same spatial location. Both the moving pattern and moving slit conditions produced the same thresholds and are, therefore, likely to use the same method of processing. This result was replicated across all observers making it unlikely to be coincidental and if they were not using the same method of processing we would expect different thresholds as one is spread across space and the other is not. We are unsure of the method involved, but it does not rely on retinotopic mapping and must involve some sort of visual memory storage.

It is interesting that the random slit condition (where a slit randomly reveals an RF pattern in a piecemeal fashion) produced lower thresholds than the moving slit and moving pattern conditions. A potential explanation for this is that for each successive frame in the moving pattern or moving slit conditions the slit progresses 3′ of visual angle. This results in 3′ of "new information," but 7′ of "old information." For the random slit condition, however, each successive frame is unlikely to be a slit which is immediately next to the previous slit. This results in more "new information" and less "old information," meaning there would be more information available to the visual system about the pattern per unit time. Without the data from Experiment 2 this would seem like a reasonable explanation; however, given those results, it would seem unlikely. Experiment 2 showed that changing the presentation time of the moving slit condition had no effect on observer thresholds. This would indicate that changing the amount of information present per unit time (in the time range assessed) does not effect sensitivity and therefore, is evidence against this potential explanation for the increased sensitivity to the random slit condition, suggesting that low-level visual effects cannot account for our data.

Another potential explanation could be the "early" identification of the object center. Models of RF coding (Poirier & Wilson, 2006) and physiological data (Pasupathy & Connor, 2001; Pasupathy & Connor, 2002) suggest the center of an object is highly important in shape perception. The random slit condition results in a presentation where the observer is likely to see portions of the stimulus that have significant spatial separation in quick succession. This presentation would result in an early and potentially more accurate identification of the object's center, compared to the moving slit and moving pattern conditions. This would enable more accurate polar coding of orientation information and could result in greater sensitivity for the random slit condition.

The results of Experiment 2 were extremely surprising, as we were expecting to encounter a temporal integration window within the presentation times tested. We measured presentation times starting at 250 ms and doubled the duration for each subsequent condition until we reached 4,000 ms. We were expecting to see either a continuous systematic change or step change in either sensitivity or integration slope when we compared across conditions. However, it is clear from the data that the presentation times tested had no effect on performance. Logically, there must be a limit to the duration over which an observer can integrate contour information; however, we were not able to find any indication of what that duration might be.

Our results are contrary to some of those presented by Bell and Corke (2014). In their second experiment they displayed each third of an RF3 (with either one, two, or three cycles of modulation) one at a time and found evidence for global integration when all three parts were presented within a 200 ms window, but not for longer durations. However, our results have suggested global processing can occur up to 4,000 ms and potentially longer. Research by Wilson and Fung (2016) provides a potential explanation. They investigated the effect of discontinuities on motion RF perception. They found that presenting a pattern as discontinuous segments increased observer thresholds by a factor of 2. Perhaps the discontinuity present in the stimulus used by Bell and Corke (2014) resulted in the visual system being unable to group the discrete segments together, disrupting global processing for longer presentation times.

Experiment 3 replicated the findings of the second experiment of Or et al. (2011), using a dot to trace out an RF pattern with a constant angular velocity. We found that by removing the speed cue created by this constant angular velocity integration slopes became

steeper and analogous to those found in Experiments 1 and 2. In fact, there was no difference between the thresholds for the moving slit, moving pattern, and constant retinal speed conditions. The current authors believe this to be evidence that the Or et al. (2011) stimulus is being processed as form rather than motion (discussed as follows).

Or et al. (2011) did compare thresholds for a constant retinal speed and constant angular velocity presentation of their stimulus; however, they only examined these effects on complete motion RFs (i.e., patterns with all cycles of modulation present) and correctly concluded that there was no significant difference in thresholds for these patterns. Our investigation of these effects extended to incompletely modulated motion RF patterns and suggests a result similar to that of Green et al. (2017), an interaction between a salient local cue and the global cue of the pattern. The salient local cue is detected first when the global signal is low, but as more cycles of modulation are added, the global signal increases and detection becomes a result of this global cue.

Further research using these dot stimuli has been conducted using fMRI (Gorbet et al., 2012) to compare the areas of activation of these stimuli (motion RF patterns) with static RF patterns, and "open motion" patterns (analogous to our motion line stimulus). They found increased activation for the motion RF patterns in areas V1, V2 , V3, V3A, MT, and STS when compared to static RF patterns and increased activation for the motion RF patterns in V1–V4 (but not MT or STS) when comparing to the open motion patterns. Gorbet et al. (2012, p. 11) also found the patterns of activity in areas V2 and V3 are predictive of the shape of the motion RF being viewed and note that these areas are involved in both shape and motion processing (Hegdé & Van Essen, 2000; Ito & Komatsu, 2004; Op de Beeck, Torfs, & Wagemans, 2008).

The similarity in performance for the motion RF, moving slit, and moving pattern conditions, suggests a common mechanism involved in the processing of these stimuli. Therefore, we considered a possibility suggested by Gorbet et al. (2014), in which "motion streaks" (Geisler, 1999) produce form information that is combined using the same mechanisms as those that underpin processing of contour-defined patterns. However, Wilkinson et al. (2016) provide evidence against this explanation, as they found no effect on observer thresholds when they changed the duration of presentation (i.e., the average speed of motion) or contrast of the dot used for their motion RF stimulus, both of which were designed to change the length of motion streaks. Therefore, it is unclear how the information is being processed early in the visual stream, but our results do suggest that integration of this motion-defined information occurs in the same manner as for contour-defined information. Perhaps, as suggested by Wilkinson et al. (2016), the motion RFs are providing a signal to higher levels of the ventral visual stream resulting in the similarity of results found between contour-defined RF patterns and motion-defined RF patterns found in the current study and by Wilkinson et al. (2016).

Evidence for the processing of both motion and static RF patterns in higher levels of the ventral visual stream comes from fMRI studies using RF patterns. Rainville, Yourganov, and Wilson (2005) found BOLD responses in lateral-occipital complex (LOC) increased with increasing deviation from circular (i.e., amplitude) for static patterns and suggested this was an indication of the integration of shape information in this region. Furthermore, Gorbet et al. (2014) found significantly more activation in LOC for low-frequency RF patterns (which demonstrate global integration) than for high frequency patterns (which demonstrate local processing). This result was found for both static and motion RF patterns, which they suggested indicates a common area of processing (Gorbet et al., 2014).

There are, however, some differences in the processing of static RF patterns and motion RF patterns. Behavioral results from Gorbet et al. (2014) found that observers were unable to discriminate between high frequency motion RFs (RF9 and RF10), but were able to do so for the same frequency static patterns. Additionally, Wilson and Fung (2016) investigated the effect of discontinuities on motion RF patterns. They found a significant increase in observer thresholds when compared to standard motion RFs of the same frequency. They presented each cycle of modulation for an RF3 and RF4 discontinuously. For example, instead of presenting the first, second, and third cycle of an RF3 in order, such that it created an unbroken presentation, they "jumped" from the end of the first cycle to the start of the third and from the end of the third to the start of the second, breaking up the pattern into components. There were two discontinuous conditions where, after presenting a full cycle of modulation, the dot jumped at either the point of maximum concavity or maximum convexity. Wilson and Fung (2016) found the greatest increase in threshold for the maximum concavity condition. This would suggest that points of concavity are more important for motion RFs than points of convexity. This result is contrary to Loffler et al. (2003) who found the largest increase in threshold when occluding points of maximum convexity.

Notwithstanding these results, there is evidence for the processing and integration of motion trajectories within the ventral visual stream. Tanaka and Yotsumoto (2016) used fMRI to investigate the areas activated when presenting motion trajectories, which produced the "wriggling motion trajectory illusion."

Multiple dots with different straight line trajectories produce the illusion of a "wriggling" motion due to the contextual effects of neighboring dots' motion. Additionally, some dots are grouped by the visual system causing the illusory percept of synchronized rotation. This illusory condition was compared to a control condition in which the straight line trajectories of the dots were allowed to collide, maintaining the perception of the straight line motion. They found the condition containing illusory motion displayed significantly more activation bilaterally in the early visual cortex and in the right fusiform area than for the motion control condition. They suggested the illusory motion trajectories were being processed in the ventral visual stream similar to continuous static contours (e.g., modulated lines). This may explain the similarity in observer thresholds for the motion RF, moving slit, and moving pattern conditions. Integration of the perceived orientation information for all three stimuli may have been occurring in the ventral visual stream and not in motion regions as originally suggested by Or et al. (2011).

For the modulated lines there was no difference in sensitivity or strength of integration for any of the conditions. Observer thresholds decreased significantly between one and two cycles, but not between two and three cycles of modulation. Tyler (1973) presented sinusoidally modulated lines (contour-defined) and found an improvement between one and two cycles of modulation but no improvement with additional cycles of modulation for patterns with a spatial frequency between 0.35 and 0.9 c/deg. Our modulated lines had a spatial frequency approximating 0.5 c/deg and therefore, our results replicate those of Tyler (1973). It appears, as suggested by Tyler (1973), that there is a spatial integration window for these patterns of approximately 2.5° of visual angle. As there appears to be no such spatial integration limit found for RF patterns (Jeffrey, Wang, & Birch, 2002; Wilkinson et al., 1998), and there was no evidence for global processing of any of the line stimuli, it appears that both motion-defined and contour-defined modulated lines and RF patterns are processed differently by the human visual system.

Schmidtmann and Kingdom (2017) suggested that a common mechanism exists for the detection of RF patterns and modulated lines. Although they report quite high goodness of fits for their model overall, they acknowledge that it underestimates some of the low RF patterns and, therefore, it is likely the high frequency RF patterns are driving their goodness of fit values. This could explain the difference between their results and those of Green et al. (2017) who found evidence that low frequency RF patterns and modulated lines are processed differently by the human visual system. Low-frequency RF patterns demonstrate global processing whereas high frequency patterns do not (Bell, Badcock, Wilson, & Wilkinson, 2007; Hess et al., 1999; Jeffrey et al., 2002; Loffler et al., 2003; Schmidtmann et al., 2012). The majority of these globally processed low frequency patterns tested by Schmidtmann and Kingdom (2017) are not adequately described by their model and, therefore, may not be generalizable to globally processed RF patterns. This conclusion is consistent in predicting the same range of RF patterns that are different to modulated lines as first noted by Wilkinson et al. (1998).

Recent work has shown a number of similarities between motion RFs and static RF patterns (Wilkinson et al., 2016). They found that thresholds increase proportional to the pattern's radius and thresholds decrease as a function of increasing RF number, which conforms to a power–law relationship, both of which have been shown for static RF patterns (Wilkinson et al., 1998). This is consistent with the suggestion that the processing of the shape of motion RF patterns also occurs in the form areas, rather than in motion areas of the visual cortex.

Keywords: shape perception, global processing, signal detection theory, RF patterns, motion RF patterns, modulated lines, probability summation, slit viewing, temporal displacement

Acknowledgments

The research was supported by Australian Research Council grants DP110104553 and DP160104211 to DRB and a UPA scholarship to RJG. Thanks to Kirsten Panton, Thomas McDougall, Serena Cribb, Hugh Riddell, and Ken Tan. Very special thanks to "Deadline" Daisy.

Commercial relationships: none.
Corresponding author: Robert J. Green.
Email: robert.green@research.uwa.edu.au.
Address: School of Psychological Science, The University of Western Australia, Perth, Australia.

References

Almeida, R. A., Dickinson, J. E., Maybery, M. T., Badcock, J. C., & Badcock, D. R. (2010). Visual search performance in the autism spectrum II: The radial frequency search task with additional segmentation cues. *Neuropsychologia*, *48*(14), 4117–4124.

Apthorp, D., Schwarzkopf, D. S., Kaul, C., Bahrami, B., Alais, D., & Rees, G. (2013). Direct evidence for

encoding of motion streaks in human visual cortex. *Proceedings of the Royal Society B: Biological Sciences*, *280*(1752), https://doi.org/10.1098/rspb.2012.2339.

Badcock, D. R., & Dickinson, J. E. (2009). Second-order orientation cues to the axis of motion. *Vision Research*, *49*(3), 407–415. https://doi.org/10.1016/j.visres.2008.11.009.

Baldwin, A. S., Schmidtmann, G., Kingdom, F. A., & Hess, R. F. (2016). Rejecting probability summation for radial frequency patterns, not so Quick! *Vision Research*, *122*, 124–134, https://doi.org/10.1016/j.visres.2016.03.003.

Baron, W. S., & Westheimer, G. (1973). Visual acuity as a function of exposure duration. *Journal of the Optical Society of America*, *63*(2), 212–219.

Bell, J., & Badcock, D. R. (2008). Luminance and contrast cues are integrated in global shape detection with contours. *Vision Research*, *48*(21), 2336–2344, https://doi.org/10.1016/j.visres.2008.07.015.

Bell, J., Badcock, D. R., Wilson, H., & Wilkinson, F. (2007). Detection of shape in radial frequency contours: Independence of local and global form information. *Vision Research*, *47*(11), 1518–1522, https://doi.org/10.1016/j.visres.2007.01.006.

Bell, J., & Corke, M. (2014). *The temporal envelope of global shape processing*. Paper presented at the Australasian Experimental Psychology Conference, Brisbane, Australia.

Bell, J., Dickinson, J. E., & Badcock, D. R. (2008). Radial frequency adaptation suggests polar-based coding of local shape cues. *Vision Research*, *48*(21), 2293–2301, https://doi.org/10.1016/j.visres.2008.07.003.

Bell, J., Sacks, G., & Burr, D. (2015). Integration times of global shape mechanisms are limited by low level processes operating prior to spatial integration. *Journal of Vision*, *15*(12): 1032, https://doi.org/10.1167/15.12.1032. [Abstract]

Bell, J., Wilkinson, F., Wilson, H. R., Loffler, G., & Badcock, D. R. (2009). Radial frequency adaptation reveals interacting contour shape channels. *Vision Research*, *49*(18), 2306–2317, https://doi.org/10.1016/j.visres.2009.06.022.

Burr, D., & Ross, J. (2004). Vision: The world through picket fences. *Current Biology*, *14*(10), R381–R382, https://doi.org/10.1016/j.cub.2004.05.011.

Burr, D., & Santoro, L. (2001). Temporal integration of optic flow, measured by contrast and coherence thresholds. *Vision Research*, *41*(15), 1891–1899, https://doi.org/10.1016/S0042-6989(01)00072-4.

Cribb, S. J., Badcock, J. C., Maybery, M. T., & Badcock, D. R. (2016). Dissociation of local and global contributions to detection of shape with age. *Journal of Experimental Psychology: Human Perception and Performance*, *42*(11), 1761–1769, https://doi.org/10.1037/xhp0000257.

Daar, M., Or, C. C. F., & Wilson, H. (2012). Increment threshold functions for radial frequency motion trajectories exhibit a dipper function above threshold. *Journal of Vision*, *12*(9): 644, https://doi.org/10.1167/12.9.644. [Abstract]

Dickinson, J. E., Bell, J., & Badcock, D. R. (2013). Near their thresholds for detection, shapes are discriminated by the angular separation of their corners. *PLoS One*, *8*(5), e66015, https://doi.org/10.1371/journal.pone.0066015.

Dickinson, J. E., Cribb, S. J., Riddell, H., & Badcock, D. R. (2015). Tolerance for local and global differences in the integration of shape information. *Journal of Vision*, *15*(3):21, 1–24, https://doi.org/10.1167/15.3.21. [PubMed] [Article]

Dickinson, J. E., Han, L., Bell, J., & Badcock, D. R. (2010). Local motion effects on form in radial frequency patterns. *Journal of Vision*, *10*(3):20, 1–15, https://doi.org/10.1167/10.3.20. [PubMed] [Article]

Dickinson, J. E., McGinty, J., Webster, K. E., & Badcock, D. R. (2012). Further evidence that local cues to shape in RF patterns are integrated globally. *Journal of Vision*, *12*(12):16, 1–17, https://doi.org/10.1167/12.12.16. [PubMed] [Article]

Felleman, D. J., & Van Essen, D. C. (1991). Distributed hierarchical processing in the primate cerebral cortex. *Cerebral Cortex*, *1*(1), 1–47.

Geisler, W. S. (1999, July 1). Motion streaks provide a spatial code for motion direction. *Nature*, *400*(6739), 65, https://doi.org/10.1038/21886.

Gorbet, D. J., Wilkinson, F., & Wilson, H. R. (2012). An fMRI examination of the neural processing of periodic motion trajectories. *Journal of Vision*, *12*(11):5, 1–15, https://doi.org/10.1167/12.11.5. [PubMed] [Article]

Gorbet, D. J., Wilkinson, F., & Wilson, H. R. (2014). Neural correlates of radial frequency trajectory perception in the human brain. *Journal of Vision*, *14*(1):11, 1–19, https://doi.org/10.1167/14.1.11. [PubMed] [Article]

Green, R. J., Dickinson, J. E., & Badcock, D. R. (2017). Global processing of random-phase radial frequency patterns but not modulated lines. *Journal of Vision*, *17*(9):18, 1–11, https://doi.org/10.1167/17.9.18. [PubMed] [Article]

Habak, C., Wilkinson, F., Zakher, B., & Wilson, H. R. (2004). Curvature population coding for complex

shapes in human vision. *Vision Research*, *44*(24), 2815–2823, https://doi.org/10.1016/j.visres.2004.06.019.

Hegdé, J., & Van Essen, D. C. (2000). Selectivity for complex shapes in primate visual area V2. *Journal of Neuroscience*, *20*(5), RC61–RC61.

Hess, R. F., Wang, Y.-Z., & Dakin, S. C. (1999). Are judgements of circularity local or global? *Vision Research*, *39*(26), 4354–4360.

Ito, M., & Komatsu, H. (2004). Representation of angles embedded within contour stimuli in area V2 of macaque monkeys. *Journal of Neuroscience*, *24*(13), 3313–3324, https://doi.org/10.1523/jneurosci.4364-03.2004.

Jeffrey, B. G., Wang, Y.-Z., & Birch, E. E. (2002). Circular contour frequency in shape discrimination. *Vision Research*, *42*(25), 2773–2779.

Kingdom, F. A., Baldwin, A. S., & Schmidtmann, G. (2015). Modeling probability and additive summation for detection across multiple mechanisms under the assumptions of signal detection theory. *Journal of Vision*, *15*(5):1, 1–16, https://doi.org/10.1167/15.5.1. [PubMed] [Article]

Kontsevich, L. L., & Tyler, C. W. (1999). Bayesian adaptive estimation of psychometric slope and threshold. *Vision Research*, *39*(16), 2729–2737.

Legge, G. E. (1978). Sustained and transient mechanisms in human vision: Temporal and spatial properties. *Vision Research*, *18*(1), 69–81.

Loffler, G., Wilson, H. R.,& Wilkinson, F. (2003). Local and global contributions to shape discrimination. *Vision Research*, *43*(5), 519–530.

Mather, G., Pavan, A., Bellacosa Marotti, R., Campana, G., & Casco, C. (2013). Interactions between motion and form processing in the human visual system. *Frontiers in Computational Neuroscience*, *7*, 65, https://doi.org/10.3389/fncom.2013.00065.

Op de Beeck, H. P., Torfs, K., & Wagemans, J. (2008). Perceived shape similarity among unfamiliar objects and the organization of the human object vision pathway. *Journal of Neuroscience*, *28*(40), 10111–10123, https://doi.org/10.1523/jneurosci.2511-08.2008.

Or, C. C.-F., Thabet, M., Wilkinson, F., & Wilson, H. R. (2011). Discrimination and identification of periodic motion trajectories. *Journal of Vision*, *11*(8):7, 1–11, https://doi.org/10.1167/11.8.7. [PubMed] [Article]

Pasupathy, A., & Connor, C. E. (2001). Shape representation in area V4: Position-specific tuning for boundary conformation. *Journal of Neurophysiology*, *86*(5), 2505–2519.

Pasupathy, A., & Connor, C. E. (2002). Population coding of shape in area V4. *Nature Neuroscience*, *5*(12), 1332–1338.

Pelli, D. G. (1985). Uncertainty explains many aspects of visual contrast detection and discrimination. *Journal of the Optical Society of America A*, *2*(9), 1508–1532.

Poirier, F. J., & Wilson, H. R. (2006). A biologically plausible model of human radial frequency perception. *Vision Research*, *46*(15), 2443–2455.

Prins, N., & Kingdom, F. A. A. (2009). *Palamedes: Matlab routines for analyzing psychophysical data*. Retrieved from http://www.palamedestoolbox.org.

Quick, R. F. (1974). A vector-magnitude model of contrast detection. *Kybernetik*, *16*(2), 65–67, https://doi.org/10.1007/bf00271628.

Rainville, S. J. M., Yourganov, G., & Wilson, H. R. (2005). Closed-contour shapes encoded through deviations from circularity in lateral-occipital complex (LOC): An fMRI study. *Journal of Vision*, *5*(8): 471, https://doi.org/10.1167/5.8.471. [Abstract]

Ross, J., Badcock, D. R., & Hayes, A. (2000). Coherent global motion in the absence of coherent velocity signals. *Current Biology*, *10*(11), 679–682.

Schmidtmann, G., Kennedy, G. J., Orbach, H. S., & Loffler, G. (2012). Non-linear global pooling in the discrimination of circular and non-circular shapes. *Vision Research*, *62*, 44–56.

Schmidtmann, G., & Kingdom, F. A. A. (2017). Nothing more than a pair of curvatures: A common mechanism for the detection of both radial and non-radial frequency patterns. *Vision Research*, *134*, 18–25. https://doi.org/10.1016/j.visres.2017.03.005.

Takemura, H., Rokem, A., Winawer, J., Yeatman, J. D., Wandell, B. A., & Pestilli, F. (2016). A major human white matter pathway between dorsal and ventral visual cortex. *Cerebral Cortex*, *26*(5), 2205–2214, https://doi.org/10.1093/cercor/bhv064.

Tan, K. W., Bowden, V. K., Dickinson, J. E., & Badcock, D. R. (2015). Modulated textures with shape structures implied by a closed flow are processed globally. *Journal of Vision*, *15*(3):17, 1–18, https://doi.org/10.1167/15.3.17. [PubMed] [Article]

Tan, K. W., Dickinson, J. E., & Badcock, D. R. (2013). Detecting shape change: Characterizing the interaction between texture-defined and contour-defined borders. *Journal of Vision*, *13*(14):12, 1–16, https://doi.org/10.1167/13.14.12. [PubMed] [Article]

Tanaka, R., & Yotsumoto, Y. (2016). Networks extending across dorsal and ventral visual pathways correlate with trajectory perception. *Journal of*

Vision, *16*(6):21, 1–14, https://doi.org/10.1167/16.6.21. [PubMed] [Article]

Tang, M. F., Dickinson, J. E., Visser, T. A. W., & Badcock, D. R. (2015). The broad orientation dependence of the motion streak aftereffect reveals interactions between form and motion neurons. *Journal of Vision*, *15*(13):4, 1–18, https://doi.org/10.1167/15.13.4. [PubMed] [Article]

Tyler, C. W. (1973). Periodic vernier acuity. *The Journal of physiology*, *228*(3), 637–647.

Van Essen, D. C., Anderson, C. H., & Felleman, D. J. (1992, January 24). Information processing in the primate visual system: An integrated systems perspective. *Science*, *255*(5043), 419.

Wilkinson, F., Haque, Y., Or, C. C.-F., Gottlieb, A. S., & Wilson, H. R. (2016). Detection of periodic motion trajectories: Effects of frequency and radius. *Journal of Vision*, *16*(7):10, 1–15, https://doi.org/10.1167/16.7.10. [PubMed] [Article]

Wilkinson, F., Wilson, H. R., & Habak, C. (1998). Detection and recognition of radial frequency patterns. *Vision Research*, *38*(22), 3555–3568, https://doi.org/10.1016/S0042-6989(98)00039-X.

Wilson, H. R., & Fung, J. (2016). Effect of motion discontinuities on discrimination of periodic trajectories. *Journal of Vision*, *16*(3):24, 1–8, https://doi.org/10.1167/16.3.24. [PubMed] [Article]

Yin, C., Shimojo, S., Moore, C., & Engel, S. A. (2002). Dynamic shape integration in extrastriate cortex. *Current Biology*, *12*(16), 1379–1385, https://doi.org/10.1016/S0960-9822(02)01071-0.